Applied Catalysis B: Environmental 142–143 (2013) 450–457

Contents lists available at SciVerse ScienceDirect

Applied Catalysis B: Environmental

journal homepage: www.elsevier.com/locate/apcatb

Synthesis of high visible light active carbon doped TiO_2 photocatalyst by a facile calcination assisted solvothermal method

Xiaoyong Wu, Shu Yin*, Qiang Dong, Chongshen Guo, Huihui Li, Takeshi Kimura, Tsugio Sato

Institute of Multidisciplinary Research for Advanced Materials, Tohoku University, 2-1-1, Katahira, Aoba-ku, Sendai 980-8577, Japan

ARTICLE INFO

Article history:
Received 2 February 2013
Received in revised form 1 May 2013
Accepted 22 May 2013
Available online 30 May 2013

Keywords:
Carbon doped TiO_2
Calcination assisted solvothermal reaction
Visible light
Photocatalytic activity

ABSTRACT

The carbon doped TiO_2 powders have been successfully prepared by a facile calcination assisted solvothermal method using titanium tetra-n-butoxide or $TiCl_3$ together with ethanol as starting materials without the addition of any other extra carbon sources. The physicochemical properties of as-synthesized samples were characterized by the X-ray diffraction, Fourier transform-infrared spectroscopy, UV–vis diffuse reflectance spectroscopy, BET specific surface area, and X-ray photoelectron spectroscopy. Besides, the effects of post solvothermal reaction heating temperature and raw materials on the carbon doping in TiO_2 have been investigated. The experimental results showed that carbon has been doped into TiO_2 lattice by replacing the oxygen site with the production of oxygen vacancy. In addition, carbon doped TiO_2 samples exhibited not only very good destruction ability of NO gas but also excellent degradation ability of methyl orange solution under the visible light much superior to P25 and N–TiO_2. The employed method in this work provided a favorable evidence that the effect of carbon doping on the properties of samples should be taken into consideration when preparing TiO_2 based photocatalyst by a hydrothermal or solvothermal method with the assist of calcination.

1. Introduction

Photocatalysis as a green chemistry technology has drawn considerable attention due to its extensively potential applications in the air purification, degradation of organic pollutant and solar energy conversion [1–5]. Although a lot of novel compounds with various photocatalytic activities have been proposed until now [6,7,4,8], TiO_2 is still the most promising photocatalyst because of its high oxidative power, abundance, chemical stability, environmentally friendly and low cost [9–11]. Unfortunately, there is a key drawback for the widespread application of TiO_2 that can only absorb UV light (about 5% of solar light) owing to its wide band gap (3.2 eV for anatase). In this case, large amounts of efforts have been devoted to extending the light absorption of TiO_2 to the visible-light region by dye sensitizing [12,13], metal doping [14,15], nonmetal doping [16,17], etc. Among these methods, nonmetal doping TiO_2 has attracted much more interest of researchers [18–21], since the dye sensitizing process is not suitable for decomposing aqueous pollutants and metal doping will increase carrier trapping in TiO_2 lattice [22].

Recently, the carbon doped TiO_2 [23–26] has received special attention after S. Sakthivel et al. reported that carbon doped particles presented five times more active than nitrogen-doped TiO_2 in the degradation of 4-chlorophenol by visible light [27]. According to the density functional theory calculations within the generalized gradient approximation reported by Valentin et al., carbon can be doped into TiO_2 lattice and then strongly enhance the visible light absorption of TiO_2 via substituting oxygen sites or getting into the interstitial positions of TiO_2, which is due to the introduction of series of localized occupied states into the band gap of TiO_2 lattice [28]. Park et al. [29] presented that high visible light induced photocatalytic performance of carbon doped TiO_2 has been successfully prepared by a conventional sol–gel synthesis. Dong et al. [30] demonstrated that mesoporous C doped TiO_2 nanomaterials with an anatase phase can be prepared by a one-pot green synthetic approach using sucrose as a carbon doping source. Irie et al. [31] reported that carbon doped anatase TiO_2 powders were obtained by oxidizing commercial TiC powders under O_2 flow at 600 °C. However, to the best of our knowledge, most of the carbon doped TiO_2 products are prepared in the presence of extra carbon raw materials (tetrabutylammonium hydroxide, sucrose, urea, glucose), high heating temperature or without consideration of effect of ethanol from the reaction solution.

Air pollution by NO_x, SO_2, CO, etc. have become more and more serious due to the use of liquefied petroleum gas cooking stoves,

* Corresponding author. Tel.: +81 22 217 5598; fax: +81 22 217 5598.
E-mail address: shuyin@tagen.tohoku.ac.jp (S. Yin).

0926-3373/$ – see front matter © 2013 Elsevier B.V. All rights reserved.
http://dx.doi.org/10.1016/j.apcatb.2013.05.052

infiltration from nearby vehicular emissions and the combustion of nitrogen gas with oxygen in the air [24]. Generally, these pollutants were mainly disposed by remediation techniques, including adsorption and filtration methods, which have very low efficiency to remove gases and also have disposal and regeneration problems. Therefore, photocatalysis as a green process would be a promising method for the disposition of poison gas [32,33].

In this study, the carbon doped TiO_2 with high visible light photocatalytic activities has been prepared by a facile calcination assisted solvothermal method using titanium tetra-n-butoxide or titanium (III) chloride and ethanol as raw materials without the addition of any other carbon precursors. Meanwhile, the effect of ethanol used as a reaction solution on the carbon doping in the TiO_2 was also studied. Furthermore, the decomposition of NO gas and degradation of methyl orange have been employed to investigate the photocatalytic activity of carbon doped TiO_2.

2. Experimental

2.1. Sample preparation

Carbon doped TiO_2 nanoparticles have been successfully prepared by a facile calcination assisted solvothermal method. In a typical solvothermal synthesis process, 13 mL titanium tetra-n-butoxide was added dropwise to 35 mL ethanol/water (30:5) mixed solution with continuous stirring for 30 min. Subsequently, the solution was transferred into a 100 mL Teflon-lined stainless steel autoclave and heated at 190 °C for 2 h. After that, the products were centrifuged, washed with distilled water and ethanol four times, respectively, followed by drying in a vacuum at 60 °C overnight. The as-prepared white precursor powder was designated as CT-BE. Then, CT-BE sample was calcined at 165, 265 and 400 °C for 1 h in a muffle furnace, and the products were designated as CT-BE-165, CT-BE-265 and CT-BE-400, respectively. For comparison, two samples were also fabricated by the similar process using titanium (III) chloride as Ti resource and different solvents, such as mixed ethanol/water (30:5) solution and pure distilled water at 190 °C for 2 h, followed by calcination at 265 °C for 1 h, and the products were designated as CT-CE-265 and T-CW-265, respectively. The sample names and concrete synthesis conditions are listed in Table 1.

2.2. Characterization

The crystalline phases of the products were identified by X-ray diffraction analysis (XRD, Bruker AXS D2 Phaser) using graphite-monochromized CuKα radiation.The UV–vis diffuse reflectance spectra (DRS) were measured out using a UV–vis spectrophotometer (Shimadazu, UV-2450). The specific surface areas were determined by the BET method (Quantachrome Instruments, NOVA4200e). The size and shape of the nanoparticles were observed by transmission electron microscopy (TEM, JEOLJEM-2010). FT-IR measurements were conducted by using the FTS7000 series (DIGILIB). The surface composition and binding energy of the samples were determined by X-ray photoelectron spectroscopy (XPS, Perkin Elmer PHI 5600). The shift of the binding energy owing to relative surface charging was corrected using the C 1s level at 284.6 eV as an internal standard and Ar^+ sputtering was employed to clean the surface of samples.

2.3. Photocatalytic activity tests

The photocatalytic activity of carbon doped TiO_2 was investigated by evaluating the decomposition of NO ($DeNO_x$) in a flow type reactor under irradiation of a 450 W high pressure mercury lamp at room temperature. The photocatalyst was spread in the hollow (20 mm × 16 mm × 0.5 mm) of a glass plate and then was placed at the bottom center of the reactor (373 cm^3 of internal volume) in which a 1:1 mixed gas of air and nitrogen containing 1 ppm of NO was flowed at the rate of 200 cm^3 min^{-1}. The sample powder was kept in the dark for 30 min to reach the adsorption and desorption equilibrium of NO gas. After that, the mercury light was turned on to irradiate the sample, where the light wavelengths were controlled by several filters: Pyrex glass for >290 nm, Kenko L41 Super Pro (W) filter >400 nm and Fuji triacetyl cellulose filter >510 nm. The measuring time for each sample under each wavelength was 10 min [26]. The concentration of NO was checked by a NO_x analyzer (Yanaco, ECL-88A).

In addition, the degradation of methyl orange (MO) was also used to characterize the photocatalytic activity of samples under the irradiation of 300 W simulated solar light (ASAHI SPECTRA HAL-302) with a 400 nm cut-off long-pass filter. The experiment was carried out at the ambient temperature. The same amount (0.05 g) of sample powder was introduced into a 50 mL of 15 mg/L MO solution. Before irradiation, the MO aqueous solution was stirred for 1 h in the dark to reach the adsorption–desorption equilibrium for MO. At the desired illumination time intervals, 5 mL suspensions were withdrawn and then centrifuged to remove the sample particles. The concentration of MO was monitored by recording the maximum absorbance of MO at 464 nm with a UV–vis spectrophotometer.

3. Results and discussion

3.1. The effect of post solvothermal heating temperature on the carbon doping in TiO_2

Fig. 1 shows the XRD patterns of C doped TiO_2 samples prepared by the solvothermal reaction followed by calcinations at different temperatures and corresponding TEM image for sample CT-BE-265. From Fig. 1(A), it can be clearly seen that all the diffraction peaks could be indexed to the anatase phase of TiO_2 (JCPDS file No. 21-1272) and no other impurity peaks were appeared. The average crystallite sizes of CT-BE, CT-BE-165, CT-BE-265 and CT-BE-400 were calculated from the full widths at half-maximum of the (1 0 1) peak according to the Scherrer equation ($D = 0.9\lambda/(\beta\cos\theta)$) as 11.5, 11.6, 11.7 and 12.2 nm, respectively, indicating the average particle of samples increased a little with the increase of post solvothermal reaction heating temperature. In addition, it could be found that the particle size of CT-BE-265 agreed well with that observed from inserted TEM image. Fig. 1(B) demonstrates the enlarged diffraction region of corresponding samples between 24 and 27°. It is apparent that when the samples were calcined at 165 and 265 °C, the (1 0 1) peak shifted a little to lower degree compared with that of sample without calcination and the corresponding lattice parameter changed from $a = 3.7917$ Å, $c = 9.5040$ Å (sample CT-BE) to $a = 3.8108$ Å, $c = 9.5432$ Å (sample CT-BE-165) and $a = 3.8197$ Å, $c = 9.5486$ Å (sample CT-BE-265). This shift may be mainly due to the carbon doping in the TiO_2 lattice, since the bond length of Ti–C (2.008 and 2.217 Å) is longer than that of Ti–O (1.942 and 2.002 Å), and the radius of C^{4-} is also larger than that of O^{2-} in the TiO_2 lattice [28]. However, when the sample was calcined at 400 °C, the position of (1 0 1) peak shifted back to the original position of the sample CT-BE. It should be assigned to the release of doped carbon from TiO_2 lattice at high temperature [29].

The diffuse reflectance spectra and corresponding Kubelka–Munk plots of CT-BE, CT-BE-165, CT-BE-265 and CT-BE-400 are displayed in Fig. 2. As shown in Fig. 2 (A), it is clear that the visible light absorption from 400 to 800 nm increased with an increase in heating temperature up to 265 °C, but decreased dramatically at 400 °C to that of CT-BE. The band gap energy of CT-BE, CT-BE-165, CT-BE-265 and CT-BE-400 were determined as 3.11,

Table 1
Detailed synthesis conditions of the samples.

Sample name	Ti source		Solvent		Calcined temperature (°C)
	Titanium tetra-n-butoxide (mL)	Titanium(III) chloride (mL)	Ethanol (mL)	Distilled Water (mL)	
CT-BE	13	0	30	5	None
CT-BE-165	13	0	30	5	165
CT-BE-265	13	0	30	5	265
CT-BE-400	13	0	30	5	400
CT-CE-265	0	10	30	5	265
T-CW-265	0	10	0	35	265

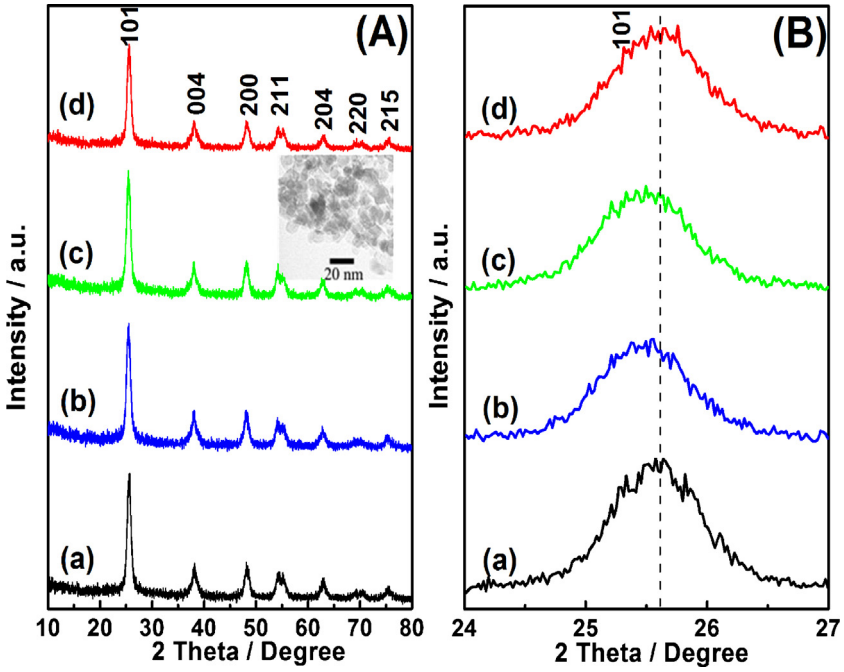

Fig. 1. (A) XRD patterns of C doped TiO_2 samples (the inset is the TEM image of CT-BE-265), (B) the amplified diffraction profiles in the range from 24 to 27°. (a) CT-BE (without calcination), (b) CT-BE-165, (c) CT-BE-265, (d) CT-BE-400.

2.78, 2.39 and 3.01 eV, respectively, by the intercept of the plots of $(\alpha h\upsilon)^{1/2}$ versus photon energy ($h\upsilon$) (in Fig. 2(B)) [6]. Meanwhile, the corresponding color of four samples changed as white, brown, deep brown and white, respectively. The enhancement of visible light absorption for CT-BE-165 and CT-BE-265 should be ascribed to the carbon doping in the TiO_2 lattice, which would introduce a series of localized occupied states into the band gap of TiO_2 lattice, leading to the strong visible light absorption [28]. As for CT-BE-400, its reflectance spectra became similar to that of CT-BE, since the doped carbon was eliminated from the TiO_2 lattice by the high temperature calcination. These light absorption profiles were nicely consistent with that of XRD results.

Fig. 3 represents the FTIR spectra of CT-BE, CT-BE-165, CT-BE-265 and CT-BE-400. The peak at about 3120 cm^{-1} is attributed to the stretching vibration mode of hydroxyls and adsorbed water, and the peak located at 1635 cm^{-1} is ascribed to bending vibration mode of O—H bond from hydroxyls and adsorbed water [34]. It can be obviously seen that when the sample was calcined at above 265 °C, the peak at 2958 cm^{-1} belonged to C—H bond disappeared, due to the decomposition of organics at the high temperatures.

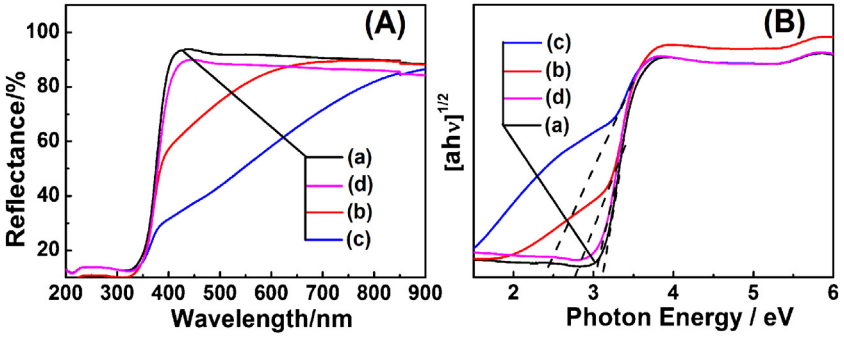

Fig. 2. (A) Diffuse reflectance spectra of (a) CT-BE (without calcination), (b) CT-BE-165, (c) CT-BE-265, (d) CT-BE-400, and (B) the Kubelka–Munk plots for the corresponding reflectance spectra of samples.

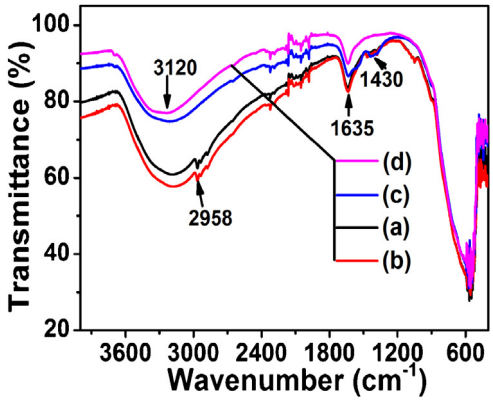

Fig. 3. The FTIR spectra of (a) CT-BE (without calcination), (b) CT-BE-165, (c) CT-BE-265 and (d) CT-BE-400.

More importantly, FTIR spectra of sample CT-BE, CT-BE-165 and CT-BE-265 had a common peak at about 1430 cm^{-1}, which can be assigned to a carbon-related substrate. However, this peak did not appear in the FTIR profile of CT-BE-400, indicating the complete decomposition of carbonaceous materials at 400 °C.

3.2. Effect of Ti source and solvent on the characteristics of TiO_2

Fig. 4 shows the XRD patterns of sample CT-BE-265, CT-CE-265 and T-CW-265 synthesized by different Ti sources and solvents followed by the calciantion at 265 °C. Although CT-BE-265 prepared using titanium tetra-n-butoxide and ethanol/water mixed solution consisted of the single phase of anatase, CT-CE-265 prepared using titanium (III) chloride and ethanol/water mixed solution consisted of a rutile/brookite mixed phase. Besides, undoped titania, T-CW-265 produced using raw materials including no carbon element, such as titanium (III) chloride and pure distilled water consisted of a pure rutile phase.

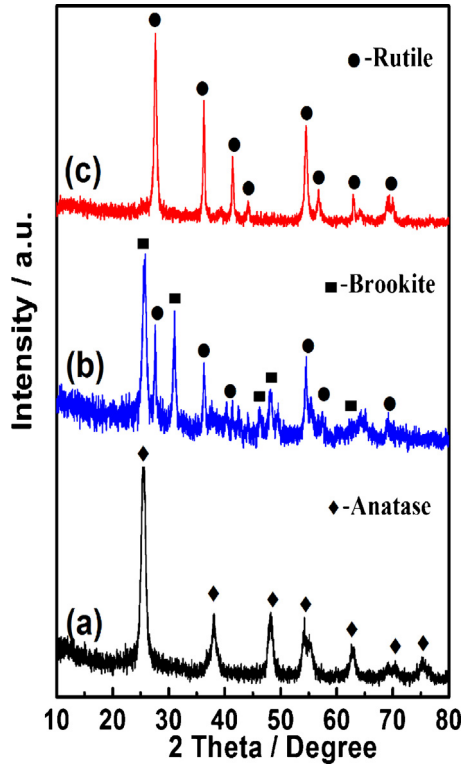

Fig. 4. XRD patterns of (a) C–TiO_2 prepared by the solvothermal reaction using titanium tetra-n-butoxide and ethanol/water mixed solution followed by calcination at 265 °C (CT-BE-265), (b) C–TiO_2 prepared by the solvothermal reaction using $TiCl_3$ and ethanol/water mixed solution followed by calcination at 265 °C (CT-CE-265), (c) undoped TiO_2 prepared by the solvothermal reaction using $TiCl_3$ and pure water followed by calcination at 265 °C (T-CW-265).

The diffuse reflectance spectra and Kubelka–Munk plots of CT-BE-265, CT-CE-265 and T-CW-265 are illustrated in Fig. 5. It could be seen that in addition to CT-BE-265 (2.39 eV), CT-CE-265 also presented nice visible light absorption with a small band gap of 2.84 eV, which was owing to carbon doping in the TiO_2 lattice. These results suggested that the doped carbon in TiO_2 can come from not only titanium tetra-butoxide used as a Ti source but also ethanol used as a solvent. As expected, the undoped titania, T-CW-265 prepared using the Ti source and solvent including no carbon element demonstrated only UV light absorption.

4. XPS analysis

The XPS measurements were employed to investigate the chemical state and binding energy of the elements for three representative samples. Fig. 6 shows the XPS survey, C 1s, O 1s and Ti 2p XPS spectra of samples CT-BE (a), CT-BE-265 (b) and CT-CE-265 (c). The peaks of C, O and Ti could be obviously seen in the survey spectrum of three samples (Fig. 6(A)). All peaks in three samples were similar except for the relative intensity. Especially, the relative intensity of C 1s increased as CT-BE < CT-CE-265 < CT-BE-265 (inset), indicating that sample CT-BE-265 contains the highest carbon.

Fig. 6(B) displays the C 1s XPS spectra of the CT-BE (a), CT-BE-265 (b) and CT-CE-265 (c). CT-BE showed three peaks at 285.6, 284.6 and 281.6 eV. The peak around 285.6 eV is attributed to the elemental carbon, which had the same binding energy as that of carbon in the graphite intercalation compound [6,35]. The peak at 284.6, which was also appeared in the samples CT-BE-265 and CT-CE-265, could be ascribed to adventitious carbon species from the XPS measurement. While the peak at 281.6 eV with low intensity is close to the C 1s peak related to the binding energy between Ti and C (281.8 eV) [26,31,36], indicating the C—Ti bond formation in the sample CT-BE. However, according to XRD, DRS results and the color of samples, it can be learned that the carbon did not doped into the inner TiO_2 lattice in the sample CT-BE. In addition, if carbon was doped into inner TiO_2 lattice, the binding energy of C—Ti should be shifted to higher energy (about 282 eV). It is well known that the electronegativity of carbon is smaller than that of oxygen. As carbon was doped into TiO_2 lattice by substituting the O site, the O—Ti—C bond would be formed, and the electron density around Ti atom should be decreased compared to that in C—Ti—C bond of TiC, which led to the shift of binding energy of C—Ti bond to higher energy. However, the binding energy of C—Ti did not shift to higher energy in the sample CT-BE [34,37,38]. Based on the above mentioned reasons, we deduced that the C—Ti bond should be formed only on the surface of sample CT-BE, which probably produced by the reaction happened between elemental carbon (285.6 eV) and surface TiO_2 during Ar^+ sputtering. The carbon concentration in the C—Ti bond of sample CT-BE was determined as 0.6 at.%. As for samples CT-BE-265 and CT-CE-265, the peak at 284.6 eV belonged to environmental carbon were also appeared but the elemental carbon peaked at 285.6 eV was disappeared in both samples, indicating that the elemental carbon in the sample had been eliminated or formed new bond with other atoms during the post solvothermal reaction calcination. Furthermore, the peak at 282 eV appeared in samples CT-BE-265 and CT-CE-265, which was also attributed to the binding energy of C—Ti bond [34,37]. According to the above explanation, from the peak at 282 eV, it could be confirmed that carbon had been successfully doped into TiO_2 lattice by forming an

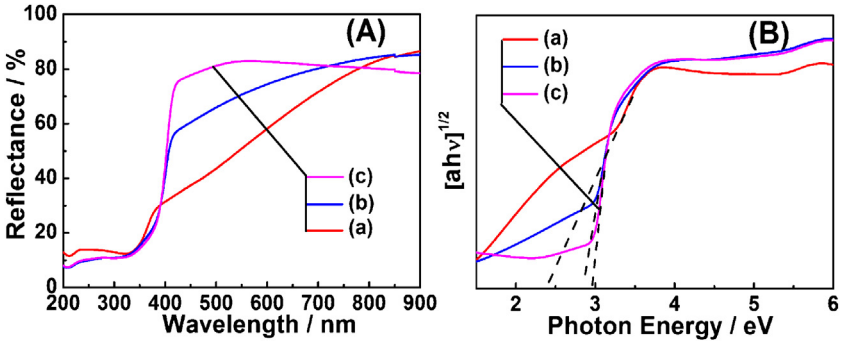

Fig. 5. (A) Diffuse reflectance spectra of (a) C–TiO_2 prepared by the solvothermal reaction using titanium tetra-n-butoxide and ethanol/water mixed solution followed by calcination at 265 °C (CT-BE-265), (b) C–TiO_2 prepared by the solvothermal reaction using $TiCl_3$ and ethanol/water mixed solution followed by calcination at 265 °C (CT-CE-265), (c) undoped TiO_2 prepared by the solvothermal reaction using $TiCl_3$ and pure water followed by calcination at 265 °C (T-CW-265), and (B) the Kubelka–Munk plots for the corresponding reflectance spectra.

O—Ti—C bond, i.e., carbon replaced the oxygen site in the TiO_2 lattice. The doped carbon concentrations in samples CT-BE-265 and CT-CE-265 were determined to be 0.42 and 0.20 at.%, respectively.

The O 1s XPS spectra of samples CT-BE, CT-BE-265 and CT-CE-265 is demonstrated in Fig. 6(C). The peak around 532.0 eV, which was assigned to OH groups [39,40], appeared in all samples. The binding energy at 530.2 eV in sample CT-BE was ascribed to Ti—O band. This peak of CT-BE-265 and CT-CE-265 shifted to higher energy of 530.6 eV, which was due to the formation of oxygen vacancies in the TiO_2 lattice [41–43]. When C^{4-} was doped

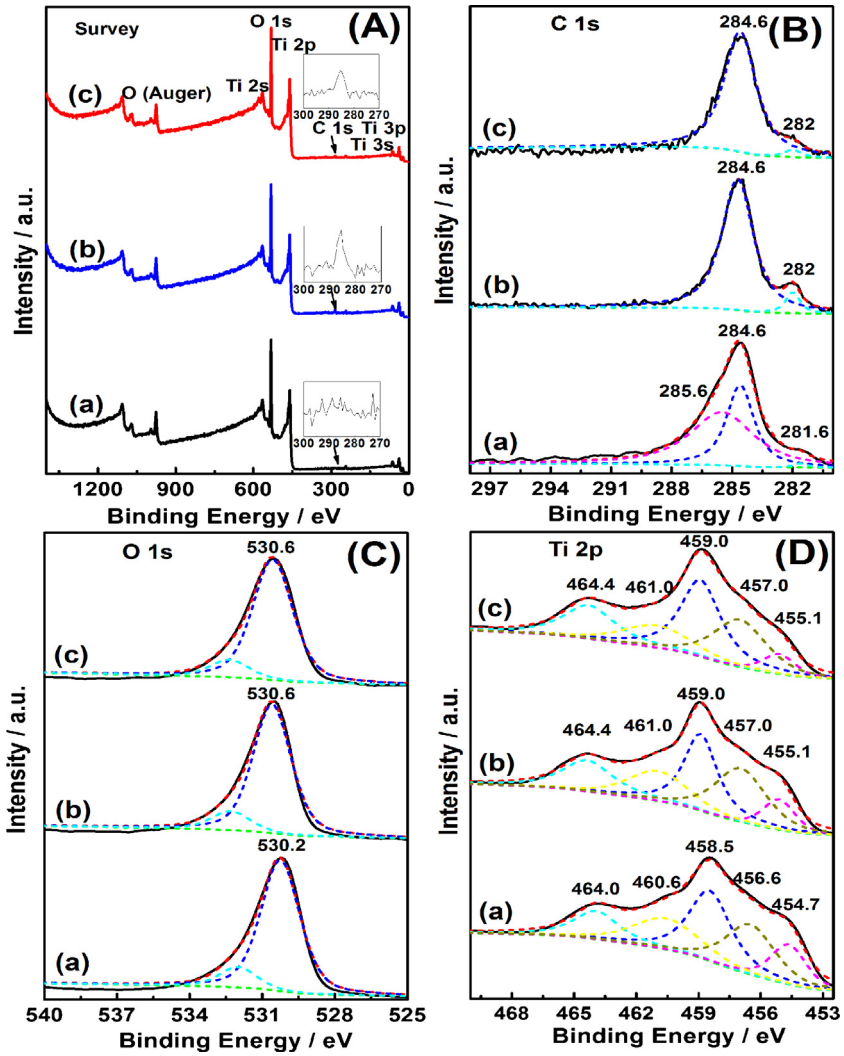

Fig. 6. The XPS spectra of (A) survey, (B) C 1s, (C) O 1s and (D) Ti 2p of (a) C–TiO_2 prepared by the solvothermal reaction using titanium tetra-n-butoxide and ethanol/water mixed solution without calcination (CT-BE), (b) C–TiO_2 prepared by the solvothermal reaction using titanium tetra-n-butoxide and ethanol/water mixed solution followed by calcination at 265 °C (CT-BE-265), (c) C–TiO_2 prepared by the solvothermal reaction using $TiCl_3$ and ethanol/water mixed solution followed by calcination at 265 °C (CT-CE-265), and the inset plots in (A) are the corresponding enlarged region of (A) from 270 to 300 eV.

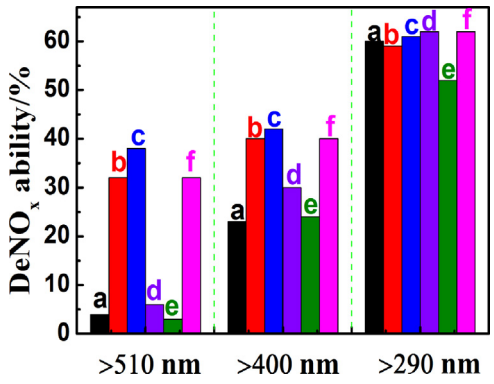

Fig. 7. DeNO$_x$ ability of CT-BE (without calcination) (a), CT-BE-165 (b), CT-BE-265 (c), CT-BE-400 (d), P25 (e) and N–TiO$_2$ (f).

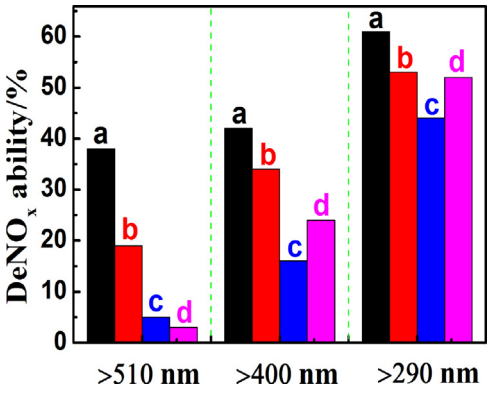

Fig. 8. DeNO$_x$ ability of C–TiO$_2$ prepared by the solvothermal reaction using titanium tetra-n-butoxide and ethanol/water mixed solution followed by calcination at 265 °C (CT-BE-265) (a), C–TiO$_2$ prepared by the solvothermal reaction using TiCl$_3$ and ethanol/water mixed solution followed by calcination at 265 °C (CT-CE-265) (b), undoped TiO$_2$ prepared by by the solvothermal reaction using TiCl$_3$ and pure water followed by calcination at 265 °C (T-CW-265) (c), and P25 (d).

into TiO$_2$ lattice by substituting O^{2-} site, some oxygen vacancies would be produced simultaneously to compensate the charge balance. Consequently, the electron density around O atoms and Ti atoms in TiO$_2$ decreased and then led to the enhancement of binding energy for O 1s and Ti 2p. Therefore, the same shift happened in the Ti 2p XPS spectra. Five peaks appeared at 454.7, 456.6, 458.5, 460.6 and 464.0 eV in sample CT-BE, which are corresponded to the binding energy of Ti^{2+}, Ti^{3+}, Ti^{4+}, Ti^{2+} and Ti^{4+} respectively. The peak positions of CT-BE-265 and CT-CE-265 shifted to 455.1, 457.0, 459.0, 461.0 and 464.4 eV (Fig. 6(D)) [44]. The appearance of Ti^{2+} and Ti^{3+} in TiO$_2$ lattice is owing to the Ar^+ sputtering during the XPS measurement [45,46].

The particle size, BET specific surface area, phase composition, band gap and C doping concentration of the samples are listed in Table 2.

4.1. Visible light induced photocatalytic activities

The photocatalytic activity test of carbon doped TiO$_2$ samples prepared by post solvothermal heating at different temperatures were investigated by the oxidative destruction of NO and the degradation of methyl orange. Fig. 7 shows the deNO$_x$ ability of samples CT-BE (a), CT-BE-165 (b), CT-BE-265 (c), CT-BE-400 (d), P25 (e) and N–TiO$_2$ (f) prepared by the conventional solvothermal method using TiCl$_3$, HMT and ethanol as raw materials, where the different wavelength lights (>510 nm, >400 nm and >290 nm) were irradiated to the samples. From Fig. 7, it can be clearly seen that the deNO$_x$ ability of sample CT-BE were about 4%, 23% and 60% under the irradiation of light wavelength >510 nm, >400 nm and >290 nm, respectively. By heating CT-BE, the visible light induced deNO$_x$ ability greatly increased, i.e., the deNO$_x$ ability of CT-BE-165 and CT-BE-265 under the irradiation of visible light (>510 nm) were 32 and 38%, respectively. This is mainly attributed to the enhancement of visible light absorption (Fig. 2) and also probably due to the effect of oxygen vacancies induced by carbon doping. Because the oxygen vacancies could introduce some defect levels between the conduction and valence band of TiO$_2$, resulting in the visible absorption of TiO$_2$ [47–50]. However, the calcination at too high temperature resulted in the decrease in the activity, i.e., the ability of CT-BE-400 was only 7% due to the elimination of doped carbon. Consequently, the sample CT-BE-265 presents the best performance for the visible light induced deNO$_x$ destruction, which is even superior to N–TiO$_2$.

The oxidative destruction of NO by sample CT-CE-265 and T-CW-265 with the comparison of CT-BE-265 and P25 is displayed in Fig. 8. It is apparent that when TiCl$_3$ was used as the Ti source instead of titanium tetra-n-butoxide, the deNO$_x$ ability under visible light (>510 nm) decreased to 19%, which is assigned to the relatively lower carbon doping concentration of CT-CE-265 compared to that of CT-BE-265. While the sample T-CW-265 showed the lowest deNO$_x$ activity because of the absence of carbon doping, i.e., poor visible light absorption ability. Therefore, it might be confirmed that the high visible light induced deNO$_x$ ability of the samples might be due to the carbon doping in the TiO$_2$ lattice, leading to the narrowing of band gap and introduction of oxygen vacancies in TiO$_2$. The stability of photocatalytic activity of sample CT-BE-265 was evaluated as shown in Fig. 9, and it was confirmed that no noticeable degradation of the photocatalytic performance was observed after three cycles.

The mechanism of deNO$_x$ reaction of carbon doped TiO$_2$ samples might be explained as follows [9,51,52]. First of all, the C–TiO$_2$ photocatalyst is irradiation by suitable light with the energy of $h\upsilon$, producing a pair of hole and electron in TiO$_2$ lattice. The photogenerated hole in the conduction band will be trapped by water in the air to generate hydroxyl radicals ·OH [53]. Meanwhile, the photoinduced electron in the valence band will form $\cdot O_2^-$ in the presence of oxygen. When NO gas flows through the surface of TiO$_2$ powders, the NO will be oxidized by ·OH, $\cdot O_2^-$ and finally transferred to HNO$_2$ or HNO$_3$ which might be easily eliminated by water (Eqs. (1)–(6)), and the corresponding schematic diagram is shown in Fig. 10. It is noteworthy that the influence of oxygen vacancies on the photocatalytic activity of TiO$_2$ as described above was not depicted in Fig. 10. However, the position of oxygen vacancy related defect levels on the band gap of TiO$_2$ are still not clarified completely yet, some researchers thought this level should

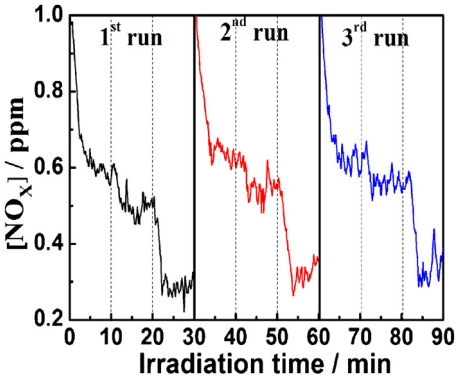

Fig. 9. The multi-cycles of deNO$_x$ ability of C–TiO$_2$ prepared by the solvothermal reaction using titanium tetra-n-butoxide and ethanol/water mixed solution followed by calcination at 265 °C (CT-BE-265).

Table 2
Particle size, BET specific surface area, phase composition, band gap and C doping concentration of the as-prepared samples.

Sample's No.	Particle Size (nm)	B.E.T. ($m^2\ g^{-1}$)	Phase	Band Gap (eV)	Doped C concentration (at%)
CT-BE	11.5	135.3	Anatase	3.11	0.06
CT-BE-165	11.6	131.5	Anatase	2.78	–
CT-BE-265	11.7	128.1	Anatase	2.39	0.42
CT-BE-400	12.2	116.6	Anatase	3.01	–
CT-CE-265	17.2	65.2	Brookite+Rutile	2.84	0.20
T-CW-265	21.6	55.3	Rutile	2.96	None

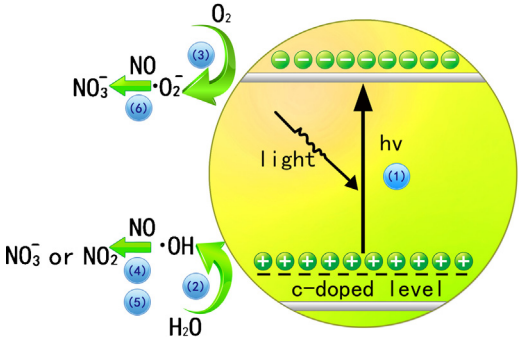

Fig. 10. Schematic illustration of the photocatalytic process on carbon doped TiO_2.

be located at the below of conduction band of TiO_2 [50,54] while others deduced this level should be situated at the above of valence band of TiO_2 [49,55]. Anywhere, small amount of oxygen vacancy would lead to the increment of visible light induced photocatalytic activity[54,56,57]. In addition, it has been reported that about 20% of NO can also be directly decomposed into N_2 and O_2 under the irradiation of light [58].

$$TiO_2 + h\upsilon \rightarrow TiO_2{*}(h^+{}_{VB} + e^-{}_{CB}) \quad (1)$$

$$h^+{}_{VB} + H_2O \rightarrow \cdot OH + H^+ \quad (2)$$

$$e^-{}_{CB} + O_2 \rightarrow \cdot O_2{}^- \quad (3)$$

$$NO + 2{\cdot}OH \rightarrow NO_2 + H_2O \quad (4)$$

$$NO_2 + \cdot OH \rightarrow NO_3{}^- + H^+ \quad (5)$$

$$NO_x + \cdot O_2{}^- \rightarrow NO_3{}^- \quad (6)$$

In addition to the deNO_x ability, the degradation of MO by CT-BE-265, P25 and N–TiO_2 as well as blank test under visible light irradiation is also shown in Fig. 11. It is explicit that the degradation of MO was due to the addition of the photocatalyst, since no noticeable destruction of MO was observed by the blank test.

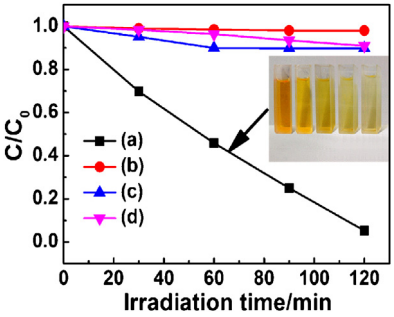

Fig. 11. The photocatalytic activity for MO degradation of C–TiO_2 prepared by the solvothermal reaction using titanium tetra-n-butoxide and ethanol/water mixed solution followed by calcination at 265 °C (CT-BE-265) (a), Blank without sample (b), P25 (c) and N–TiO_2 (d) (light source $\lambda > 400$ nm).

Furthermore, The MO had been degraded about 98% by sample CT-BE-265 within 120 min under the visible light (>400 nm), which is much higher than that of P25 and N–TiO_2. The color change of corresponding MO solution was also displayed in the inset. It implies that the carbon doped TiO_2 samples presented very good destruction ability on not only NO gas but also MO solution, being much superior to P25 and N–TiO_2.

5. Conclusions

The carbon doped TiO_2 powders was successfully prepared by a facile solvothermal reaction followed by calcination. The experimental results showed that the doped carbon could come from not only titanium tetra-n-butoxide but also ethanol in reaction solvent. Besides, the XRD, DRS and XPS results confirmed that the carbon was doped into TiO_2 lattice by substituted the oxygen site with the production of oxygen vacancies, leading to the high visible absorption of as-synthesized samples. In addition, carbon doped TiO_2 samples presented very excellent destruction ability on NO gas and MO solution under the irradiation of visible light much superior to P25 and N–TiO_2. The above described carbon doping method in TiO_2 would introduce a good way for fabrication of high visible light induced photocatalytic activity of TiO_2 for the practical application.

Acknowledgment

This research was supported in part by the Management Expenses Grants for National Universities Corporations from the Ministry of Education, Culture, Sports, Science for Technology of Japan (MEXT), and by the Grant-in-Aid for Science Research (No. 22651022, No. 23241025 & No. 25289245), the TAGEN Project, Tohoku University.

References

[1] S.C. Roy, O.K. Varghese, M. Paulose, C.A. Grimes, ACS Nano 4 (2010) 1259.
[2] S. Livraghi, M.C. Paganini, E. Giamello, A. Selloni, C. Divalentin, G. Pacchioni, Journal of the American Chemical Society 128 (2006) 15666.
[3] M. Gratzel, Nature 414 (2001) 338.
[4] J. Wang, S. Yin, Q. Zhang, F. Saito, T. Sato, Journal of Materials Chemistry 13 (2003) 2348.
[5] H.H. Li, S. Yin, T. Sato, Applied Catalysis B: Environmental 106 (2011) 586.
[6] C. Chen, M.C. Long, H. Zeng, W.M. Cai, B.X. Zhou, J.Y. Zhang, Y.H. Wu, D.W. Ding, D.Y. Wu, Journal of Molecular Catalysis A: Chemical 314 (2009) 35.
[7] T.F. Long, X.L. Dong, X.W. Liu, J.X. Liu, S. Yin, T. Sato, Research on Chemical Intermediates 36 (2010) 61.
[8] A.K. Bhattacharya, K.K. Mallick, A. Hartridge, Materials Letters 30 (1997) 7.
[9] S. Yin, B. Liu, P.L. Zhang, T. Morikawa, K. Yamanaka, T. Sato, Journal of Physical Chemistry C 112 (2008) 12425.
[10] S.U.M. Khan, M. Al-Shahry, W.B. Ingler Jr., Science 297 (2002) 2243.
[11] S. Yin, Q. Zhang, F. Saito, T. Sato, Chemistry Letters 32 (2003) 358.
[12] L. Ziolkowski, K. Vinodgopal, P.V. Kamat, Langumuir 13 (1997) 3124.
[13] D. Duonghong, E. Borgarello, M. Gratzel, Journal of the American Chemical Society 103 (1981) 4685.
[14] C. Wang, D.W. Bahnemann, J.K. Dohrmann, Chemical Communications 16 (2000) 1539.
[15] E. Bae, W. Choi, Environmental Science & Technology 37 (2003) 147.
[16] S. Yin, Y. Aita, M. Komatsu, J.S. Wang, Q. Tang, T. Sato, Journal of Materials Chemistry 15 (2005) 674.
[17] T. Ohno, T. Tsubota, K. Nishijima, Z. Miyamoto, Chemistry Letters 33 (2004) 750.
[18] D. Chen, D. Yang, Q. Wang, Z.Y. Jiang, Industrial & Engineering Chemistry Research 45 (2006) 4110.

[19] D. Li, H. Haneda, N.K. Labhsetwar, S. Hishita, N. Ohashi, Chemical Physics Letters 401 (2005) 579.
[20] S. In, A. Orlov, R. Berg, F. Garcia, S. Pedrosa-Jimenez, M.S. Tikhov, D.S. Wright, R.M. Lambert, Journal of the American Chemical Society 129 (2007) 13790.
[21] Z. Li, X.F. Chen, X.C. Wang, Y.J. Zhang, W. Wei, Y.H. Sun, M. Antonietti, M.M. Titirici, Advanced Materials 22 (2010) 3317.
[22] D. Dvoranova, V. Brezova, M. Mazur, M.A. Malati, Applied Catalysis B: Environmental 37 (2002) 91.
[23] W. Ren, Z. Ai, F. Jia, L. Zhang, X. Fan, Z. Zou, Applied Catalysis B: Environmental 69 (2007) 138.
[24] Y. Huang, W. Ho, S. Lee, L.Z. Zhang, G. Li, J.C. Yu, Langmuir 24 (2008) 3510.
[25] X. Wang, S. Meng, X. Zhang, H. Wang, W. Zhong, Q. Du, Chemical Physics Letters 444 (2007) 292.
[26] S. Yin, M. Komatsu, Q.W. Zhang, F. Saito, T. Sato, Journal of Materials Science 42 (2007) 2399.
[27] S. Sakthivel, H. Kisch, Angewandte Chemie International Edition 42 (2003) 4908.
[28] C.D. Valentin, G. Pacchioni, A. Selloni, Chemistry of Materials 17 (2005) 6656.
[29] Y. Park, W. Kim, H. Park, T. Tachikawa, T. Majima, W. Choi, Applied Catalysis B: Environmental 91 (2009) 355.
[30] F. Dong, S. Guo, H.Q. Wang, X.F. Li, Z.B. Wu, Journal of Physical Chemistry C 111 (2007) 17601.
[31] H. Irie, Y. Watanabe, K. Hashimoto, Chemistry Letters 32 (2003) 772.
[32] C.H. Ao, S.C. Lee, C.L. Mak, L.Y. Chan, Applied Catalysis B: Environmental 42 (2003) 119.
[33] H.H. Li, S. Yin, Y.H. Wang, T. Sato, Journal of Catalysis 286 (2012) 273.
[34] D.H. Wang, L. Jia, X.L. Wu, L.Q. Lu, A.W. Xu, Nanoscale 4 (2012) 576.
[35] B. Neumann, P. Bogdanoff, H. Tributsch, S. Sakthivel, H. Kisch, Journal of Physical Chemistry B 109 (2005) 16579.
[36] X.X. Wang, S. Meng, X.L. Zhang, H.T. Wang, W. Zhong, Q.G. Du, Chemical Physics Letters 444 (2007) 292.
[37] F. Dong, S. Guo, H.Q. Wang, X.F. Li, Z.B. Wu, Journal of Physical Chemistry C 115 (2011) 13285.
[38] V. Etacheri, M.K. Seery, S.J. Hinder, S.C. Pillai, Chemistry of Materials 22 (2010) 3843.
[39] J.G. Yu, G.H. Wang, B. Cheng, M.H. Zhou, Applied Catalysis B 69 (2007) 171.
[40] F.Z. Jia, Z.P. Yao, Z.H. Jiang, C.X. Li, Catalysis Communications 12 (2011) 497.
[41] X.B. Chen, C. Burda, Journal of Physical Chemistry B 108 (2004) 15446.
[42] A.E.C. Palmqvist, M. Wirde, U. Gelius, M. Muhammed, Nanostructured Materials 11 (1999) 995.
[43] R.K. Singhal, A. Samariya, S. Kumar, Y.T. Xing, D.C. jain, S.N. Dolia, U.P. Deshpande, T. Shripathi, E.B. Saitovitch, Journal of Applied Physics 107 (2010) 113916.
[44] E.Y. Wu, K.L. Ou, S.F. Ou, K.D. Jandt, Y.N. Pan, Materials Transactions 50 (2009) 891.
[45] R. Beranek, H. Kisch, Photochemical & Photobiological Sciences 7 (2008) 40.
[46] F. Zhang, S. Jin, Y. Mao, Z. Zheng, Y. Chen, X. Liu, Thin Solid Films 310 (1997) 29.
[47] J.Y. Zhang, Z.Y. Zhao, X.Y. Wang, T. Yu, J. Guan, Z.T. Yu, Z.S. Li, Z.G. Zou, Journal of Physical Chemistry C 114 (2010) 18396.
[48] A.K. Rumiz, J.C. Woicik, E. Cockayen, H.Y. lin, G.H. Jaffari, S.I. Shah, Applied Physics Letters 95 (2009) 262111.
[49] H.H. Li, S. Yin, Y.H. Wang, T. Sekino, S.W. Lee, T. Sato, Journal of Catalysis 297 (2013) 65.
[50] X.Y. Pan, M.Q. Yang, X.Z. Fu, N. Zhang, Y.J. Xu, Nanoscale 5 (2013) 3601.
[51] J.S. Dalton, P.A. Janes, N.G. Jones, J.A. Nicholson, K.R. Halam, G.C. Allen, Environmental Pollution 120 (2002) 415.
[52] Q.P. Wu, R.V.D. Krol, Journal of the American Chemical Society 134 (2012) 9369.
[53] M.R. Hoffmann, S.T. Martin, W. Choi, D.W. Bahnemann, Chemical Reviews 95 (1995) 69.
[54] I. Justicia, P. OrdejÓn, G. Canto, J.L. Mozos, J. Fraxedas, G.A. Battiston, R. Gerbasi, A. Figueras, Advanced Materials 14 (2002) 1399.
[55] A.K. Rumaiz, J.C. Woicik, E. Cockayne, H.Y. Lin, G.H. Jaffari, S.I. Shah, Applied Physics Letters 95 (2009) 262111.
[56] U. Sulaeman, S. Yin, T. Sato, Applied Physics Letters 97 (2010) 103102 (3 pages).
[57] S. Yin, U. Sulaeman, T. Sato, Materials Focus 1 (2012) 18–31.
[58] M. Anpo, NTS: Tokyo, 2002, p 9. JP803371S.